Remote Mutations Alter Transition-State Structure of Human Purine Nucleoside Phosphorylase†

Minkui Luo,‡ Lei Li,‡ and Vern L. Schramm*

Department of Biochemistry, Albert Einstein College of Medicine, 1300 Morris Park Avenue, Bronx, New York 10461

Received October 23, 2007; Revised Manuscript Received December 4, 2007

ABSTRACT: Purine nucleoside phosphorylase (PNP) catalyzes the reversible phosphorolysis of purine (2′-deoxy)ribonucleosides to give the corresponding purine base and (2′-deoxy)ribose 1-phosphate as products. Human and bovine PNPs (HsPNP and BtPNP) form distinct transition states despite 87% identity in amino acid sequence. A PNP hybrid was produced by replacing K22 and H104 in HsPNP with the corresponding Glu and Arg residues found in BtPNP. We solved the transition-state structure of E:R-HsPNP (K22E:H104R mutant of HsPNP) using competitive kinetic isotope effects (KIE) and global density functional calculations. An array of PNP transition states was generated from optimized structure candidates with varied C1′−N9, C1′−$O^{phosphate}$ distances, ribosyl pucker configurations and N7-protonation states. Isotopically labeled [1′-^{3}H], [2′-^{3}H], [1′-^{14}C], [9-^{15}N], [1′-^{14}C, 9-^{15}N] and [5′-$^3H_2$]inosines gave intrinsic KIE values of 1.210, 1.075, 1.035, 1.024, 1.065, 1.063 with E:R-HsPNP, respectively. The suite of E:R-HsPNP KIEs match a single structure from the array of PNP transition-state candidates. The transition state of E:R-HsPNP is fully dissociative, N7-protonated hypoxanthine (C1′−N9 distance ≥ 3.0 Å) with partial participation of phosphate (C1′−$O^{phosphate}$ distance = 2.26 Å), 2′-C-*exo*-ribosyl ring pucker and the O5′−C5′−C4′−O4′ dihedral angle near 60°. The transition state of E:R-HsPNP is altered from the fully dissociative D_N*A_N character for HsPNP to a late phosphate-associative character. E:R-HsPNP differs from native HsPNP by only two residues over 25 Å away from the active site. New interactions caused by the mutations increase the catalytic efficiency of the enzyme for formation of a late transition state with increased participation of the phosphate nucleophile. Dynamic coupling motions from the remote mutations to the catalytic sites are proposed.

Purine nucleoside phosphorylase (PNP) catalyzes the reversible phosphorolysis of purine (2′-deoxy)ribonucleosides to give the corresponding purine and (2′-deoxy)ribose 1-phosphate (Figure 1) (*1*). Human PNP (HsPNP[1]) is involved in the removal of deoxyguanosine (dGuo), and this process is essential for T-cell immune functions (*2, 3*). The genetic deficiency of HsPNP has been shown to cause specific T-cell immune deficiency (*4*). The syndrome results from the increased blood levels of dGuo and its conversion to dGTP in dividing T-cells. Altered deoxynucleotide pools allosterically block ribonucleotide diphosphate reductase, introduce errors into DNA and trigger apoptosis in dividing T-cells (*4, 5*). This response to dGuo has made HsPNP a target for T-cell leukemia and T-cell related autoimmune diseases (*6*−*8*). Three generations of PNP transition state analogue inhibitors have been developed and show promising therapeutic activities against resistant T-cell leukemia, cutaneous T-cell leukemia, and T-cell autoimmune disorders (*6, 9*−*15*).

The mechanism of PNP-catalyzed phosphorolysis from spectroscopic studies, transition-state analyses and crystal structure data are consistent with a stepwise "nucleophilic displacement by electrophile migration" mechanism (Figure 1) (*16*−*25*). In this mechanism, the first step is the dissociation of the ribosyl anomeric carbon from the purine base, followed by the formation of a ribooxacarbenium ion transition state (or intermediate) and migration of the ribosyl anomeric carbon toward the phosphate nucleophile to give ribose 1-phosphate as product. On the basis of chemical rate-limiting steps of PNP-catalyzed phosphorolysis, PNP reaction mechanisms can be further defined as partially dissociative $D_N^{‡}$*A_N, fully dissociative D_N*A_N (S_N1) or associative D_N*$A_N^{‡}$ with individual transition states in this order along the reaction profile (Figure 1) similar to those proposed for the hydrolysis of deoxyadenosine monophosphate (*26*).[2] The transition states of HsPNP and BtPNP are distinguished from each other by the completely dissociative D_N*A_N character for the former and the partially dissociative $D_N^{‡}$*A_N characters of the later (*21*, *22*).

HsPNP and BtPNP show 87% sequence identity with fully conserved residues at the enzyme active sites (*10*, *11*, *21*, *22*). Both HsPNP (Figure 2) and BtPNP are homotrimers with the catalytic sites located near subunit interfaces (*24*,

† Supported by NIH Research Grants GM41916 and GM068036.

* Author to whom correspondence should be addressed. E-mail: vern@aecom.yu.edu. Tel: (718) 430-2813. Fax: 718-430-8565.

‡ These authors made equal contributions.

[1] Abbreviations: HsPNP and BtPNP, human and bovine purine nucleoside phosphorylases, respectively; E:R-HsPNP, mutated form of human PNP in which Lys22 and His104 are substituted with Glu and Arg, respectively (K22E and H104R); KIE, kinetic isotope effect.

[2] See ref *26* for nomenclature of $D_N^{‡}$*A_N, D_N*A_N (S_N1) and D_N*$A_N^{‡}$ transition states.

10.1021/bi702133x CCC: $40.75
Published on Web 02/19/2008

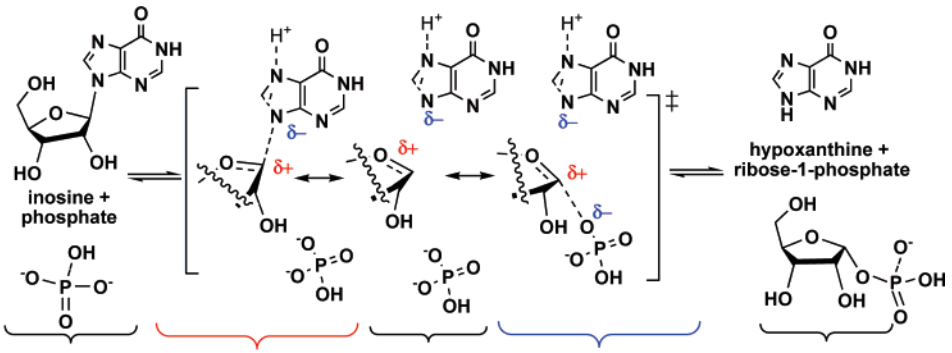

C1′-N9	1.46 Å	< 2.3 Å	2.3 - 3.0 Å	≥ 3.0 Å	≥ 3.0 Å	≥ 3.0 Å	N.A
C1′-$O^{phosphate}$	N.A	≥ 2.8 Å	≥ 2.8 Å	≥ 2.8 Å	2.8 - 2.2 Å	< 2.2 Å	1.44 Å
[1′-^{14}C] KIE	1.00	1.01 - 1.06	1.06 - 1.01	unity	1.01 - 1.06	1.06 - 1.01	1.00

FIGURE 1: Mechanism of PNP-catalyzed phosphorolysis. Inosine phosphorolysis follows a "nucleophilic displacement by electrophile migration" pathway, which involves stepwise C1′−N9 dissociation, ribooxacarbenium ion formation and C1′−$O^{phosphate}$ association to give hypoxanthine and ribose 1-phosphate as products. $D_N{}^{\ddagger *}A_N$, $D_N{}^{*}A_N$ and $D_N{}^{*}A_N{}^{\ddagger}$ represent the three mechanisms for which the rate-limiting chemical steps are C1′−N9 bond breaking, ribooxacarbenium formation and C1′−$O^{phosphate}$ bond formation, respectively. These transition states are defined according to C1′−N9 and C1′−$O^{phosphate}$ bond distances as well as the magnitude of the corresponding [1′-^{14}C] KIE values.

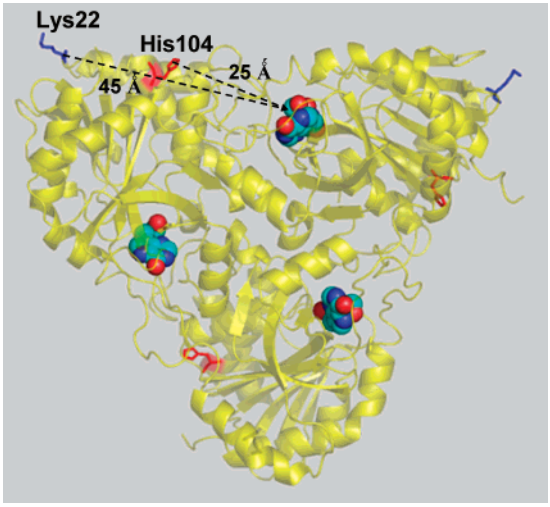

FIGURE 2: Crystal structure of human PNP trimer with K22 and H104 residues highlighted and the catalytic sites filled with immucillin-H, a transition-state analogue. The catalytic sites are located near the subunit interface. K22 and H104 are located at 45 Å and 25 Å away from the enzyme active site, respectively. The structure is taken from PDB file 1PF7.

25, *27*−*29*). E:R-HsPNP is a bovinized HsPNP in which the K22 and H104 of HsPNP were replaced with the counterparts from BtPNP. E:R-HsPNP was designed in attempts to improve crystallographic packing properties for HsPNP. While its crystallographic properties were unchanged, the enzyme exhibited altered catalytic properties (*30*). Here we show that the enzyme also displays altered transition-state structure. These mutations are located on the HsPNP outer surface and are removed from the enzyme active site by at least 25 Å (Figure 2). However, E:R-HsPNP exhibited characteristic pre-steady-state kinetics that differ from both HsPNP and BtPNP (*30*). Computational modeling also indicates that the remote E:R mutations of HsPNP can facilitate phosphorolysis via promoting vibrations into the enzyme active site.[3] This evidence suggests that the remote E:R mutation might affect the transition-state structure of PNP-catalyzed phosphorolysis.

Kinetic isotope effects (KIEs) have been used for studying kinetics (*31*), chemical equilibria (*32*), vibrational mode relaxations (*33*), tunneling (*34*), hyperconjugations, (*35*, *36*), and ionization (*37*). KIEs are particularly valuable for probing enzymatic transition states (*38*−*41*). Iteratively matched KIEs provide a boundary condition for solving the transition-state structure derived from computational modeling (*38*, *41*−*43*). The combined efficiency of KIEs and structural modeling for enzyme transition-state characterization led us to solve the transition state of E:R-HsPNP for comparison with HsPNP and BtPNP.

We explored an array of optimized candidates for PNP transition states with systematic alteration of N-ribosidic and $O^{phosphate}$-ribosidic bond distances as well as N7-protonation state, ribosyl configuration and C5′-OH conformation. The array of PNP transition-state candidates predicted characteristic KIEs at the H1′, H2′, H5′, C1′, and N9 positions. [1′-^{3}H], [2′-^{3}H], [5′-$^{3}H_2$], [1′-^{14}C], [9-^{15}N], and [1′-^{14}C, 9-^{15}N] intrinsic KIEs of E:R-HsPNP were measured experimentally and compared to the predicted KIEs from the PNP transition-state candidates. E:R-HsPNP adopts an early associative $D_N{}^{*}A_N{}^{\ddagger}$ transition state with complete dissociation of hypoxanthine and significant phosphate nucleophilic participation. Transition-state analysis, together with pre-steady-state kinetics, indicate that the K22E/H104R mutations facilitate C1′−N7 bond breaking and cause C1′−$O^{phosphate}$ bond association at the transition state.

EXPERIMENTAL PROCEDURES

Reagents and Materials. [1′-^{3}H]Ribose, [1′-^{14}C]ribose, D-[6-$^{3}H_2$]glucose 1-phosphate, and D-[6-^{14}C]glucose were purchased from American Radiolabeled Chemicals Inc.

[3] Saen-Oon, S., Ghanem, M., Wing, C., Schramm, V. L. and Schwartz, S. D. (2008) *Biophys. J. 94*, in press.

[9-^{15}N]Adenine and [2′-^{3}H]ribose were synthesized according to reported procedures (*22*, *44*). Hexokinase, glucose-6-phosphate dehydrogenase, phosphogluconic acid dehydrogenase, L-glutamic dehydrogenase, phosphoriboisomerase, adenylate kinase (AK), and pyruvate kinase (PK) were purchased from Sigma. Alkaline phosphatase was purchased from Roche. Phospho-D-ribosyl-1-pyrophosphate (PRPP) synthase, adenine phosphoribosyltransferase (APRTase) and *Plasmodium falciparum* adenosine deaminase (ADA) were purified according to the reported methods (*38*, *39*, *45*). Ribokinase (RK) was obtained as described previously (*38*, *39*). All other reagents were purchased from readily available commercial sources and used without further purification.

Computational Modeling of PNP Transition States. Transition states for the phosphorolysis of inosine were determined *in vacuo* using hybrid density functional B3LYP/6-31G (d, p) basis implemented in Gaussian 98 (*46*). A global approach was carried out to locate the best match to the intrinsic KIEs. Bond distances were systematically altered between the ribosyl anomeric carbon, hypoxanthine and phosphate (C1′−N9 and C1′−O^{phosphate}) at the transition state between inosine and α-D-ribose 1-phosphate. For transition-state structures involving hypoxanthine dissociation, the C2′−C1′−N9−C2 dihedral angle was restricted to be 41° based on the dihedral angle of 9-deazahypoxanthine in the HsPNP crystal structure with immucillin-H (*47*). The C5′-OH configuration of inosine at the transition state of HsPNP was applied to E:R-HsPNP because both enzymes report the same [5′-$^{3}H_2$] KIE of 1.062 (see Results and Discussion) (*22*, *47*). Approximately 60 structures were optimized as PNP transition-state candidates with varied C1′−N9 or C1′−O^{phosphate} distances, ribosyl pucker configurations and N7-protonation states. These transition-state structures contain partial bonds to either hypoxanthine or phosphate groups to satisfy the "nucleophilic displacement by electrophile migration" mechanism in Figure 1. The structures of inosine (substrate) and α-D-ribose 1-phosphate (product) were optimized without adding constraints. The bond frequencies for the substrate and PNP transition states were calculated using the same level of theory. All $3N - 6$ vibrational modes were used for calculating KIEs or equilibrium isotope effects (BIE, where no or $<50i$ cm^{-1} imaginary frequency was assumed) using the ISOEFF98 program (*48*). Frequencies for the substrate, the transition states and a reaction-coordinate imaginary frequency of 50i cm^{-1} or greater were used as the inputs for transition states with C1′ motion in the reaction coordinate. The KIEs or BIEs calculated by this procedure were compared with the intrinsic KIEs (see the methods below) to establish the E:R-HsPNP transition-state structure. Pauling bond orders were calculated on the basis of the equation ($r_n = r_1 - 0.3 \ln n$) as described previously (*49*), and the corresponding bond distances in the optimized substrate or product structures were used for the term r_1 in this equation.

Calculations of Molecular Electrostatic Potential Surfaces. The CUBE subprogram of Gaussian 98 was used for calculating molecular electrostatic potential (MEP) surfaces of PNP transition states. The formatted checkpoint files used in the CUBE subprogram were generated by geometry optimization at the B3LYP/6-31G (d, p) level. The MEP surfaces were visualized using Molekel 4.0 at a density of 0.2 electron/Å^3.

Scheme 1: Synthesis of Isotopically Labeled Inosines[a]

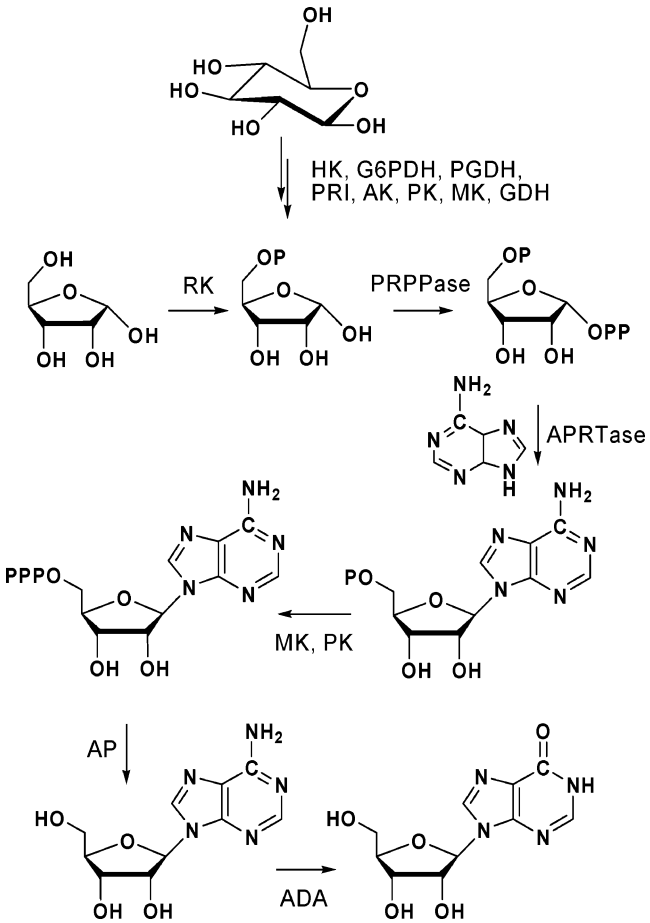

[a] [1′-^{3}H], [2′-^{3}H], [5′-$^{3}H_2$], [1′-^{14}C], [5′-^{14}C], [5′-^{14}C, 9-^{15}N], and [1′-^{14}C, 9-^{15}N]-labeled inosines were prepared from isotopically labeled riboses, glucoses and adenines through one-pot, stepwise enzymatic reactions. All radiolabeled materials were converted into adenosine triphosphates (ATP) as the first step, then adenosines and finally inosines as described in Experimental Procedures. The enzymes used for the conversion include ribokinase (RK), hexokinase (HK), glucose-6-phosphate dehydrogenase (G6PDH), phosphogluconic acid dehydrogenase (PGDH), L-glutamic acid dehydrogenase (GDH), phosphoriboisomerase (PRI), adenylate kinase (AK), pyruvate kinase (PK), alkaline phosphatase (AP), phospho-D-ribosyl-1-pyrophosphate synthase (PRPPase), adenine phosphoribosyltransferase (APRTase) and adenosine deaminase (ADA).

Synthesis of Isotopically Labeled Inosines. [1′-^{3}H], [2′-^{3}H], [5′-$^{3}H_2$], [1′-^{14}C], [5′-^{14}C], [5′-^{14}C, 9-^{15}N], and [1′-^{14}C, 9-^{15}N]-labeled inosines were prepared enzymatically from isotopically labeled riboses, glucoses and adenines as described previously with some modifications (Scheme 1) (*22*, *38*, *39*, *49*). For this approach, all radiolabeled materials were converted into adenosine triphosphates (ATP) at the first stage, then adenosines and finally inosines via three-step enzymatic reactions (Scheme 1). Briefly, 2 mM adenine and 1 mM ribose (final concentrations) were added into a solution containing 20 mM phosphoenolpyruvate, 0.1 mM ATP, 100 mM phosphate, 50 mM glycylglycine, 50 mM KCl, 20 mM $MgCl_2$ and 2 mM DTT (pH = 7.4). The reaction was initialized by the addition of an enzyme stock containing 0.01 unit ribokinase, 0.01 unit adenine phosphoribosyltransferase, 0.01 unit phospho-D-ribosyl-1-pyrophosphate synthase, 1 unit adenylate kinase and 1 unit pyruvate kinase. The mixture was incubated at 37 °C for 12 h to generate radiolabeled ATPs and heated to 95 °C for 3 min. Into this

solution, 5 mM glucose, 4 units of hexokinase, 5 units of adenylate kinase and 10 units of alkaline phosphatase were added. The reaction mixture was incubated at 25 °C for 6 h to convert ATP to adenosine. The isotopically labeled adenosines were purified by reverse phase HPLC (C-18 Deltapak column, 7.5% MeOH/H_2O, 1 mL/min). The peak eluting at 260 nm corresponded to adenosine (retention time = 14 min). Solvent was removed by speedvac to give adenosines with 90% yield on the basis of starting riboses. The adenosines were redissolved into buffer containing 20 mM phosphate and 1 μM EDTA (pH = 7.0) and quantitatively converted into [1′-^{3}H], [1′-^{14}C] and [1′-^{14}C, 9-^{15}N]-labeled inosines in 5 h at 25 °C by ADA-catalyzed deamination (1 mL reaction, 0.1 μM enzyme). Inosines were purified by reverse phase HPLC (C-18 Deltapak column, 5% MeOH/H_2O, 1 mL/min, retention time = 8 min). For preparing [5′-$^3H_2$], [5′-^{14}C] and [5′-^{14}C, 9-^{15}N]-labeled inosines, D-[6-$^3H_2$]glucose 1-phosphate and D-[6-^{14}C]glucose were converted to ATP, then to adenosine and inosine as described above. Here the reactions contain 2 mM adenine and 1 mM glucose or glucose 1-phosphate, 20 mM phosphoenolpyruvate, 0.1 mM cold ATP, 100 μM β-nicotinamide adenine dinucleotide phosphate sodium salt, 20 mM α-ketoglutarate, 5 mM NH_4Cl, 100 mM phosphate, 50 mM glycylglycine, 50 mM KCl, 20 mM $MgCl_2$ and 2 mM DTT (pH = 7.4), 1 unit of hexokinase, 1 unit of glucose-6-phosphate dehydrogenase, 0.075 unit of phosphogluconic acid dehydrogenase, 1 of unit L-glutamate dehydrogenase, 0.05 unit of phosphoriboisomerase, 0.2 unit of adenine phosphoribosyltransferase, 0.015 unit of phospho-D-ribosyl-1-pyrophosphate synthase, 1 unit of adenylate kinase and 1 unit of pyruvate kinase.

Expression and Purification of E:R-HsPNP. E:R-HsPNP was prepared by site directed mutagenesis as described earlier (*22*, *30*, *47*). Activity of E:R-HsPNP was monitored by the coupled conversion of hypoxanthine to uric acid ($\Delta\epsilon_{293}$ = 12.9 mM^{-1} cm^{-1}) at 25 °C (0.06 unit of xanthine oxidase, 50 mM potassium phosphate at pH = 7.4, varied concentration of inosine).

Determination of KIEs by Isotope Ratio Analysis. E:R-HsPNP-catalyzed arsenolysis reactions were carried out at 25 °C in a buffer containing 100 mM sodium arsenate, 50 mM Tris-HCl (pH = 7.5) and total 250 μM inosine unless indicated otherwise. For PNP, arsenate mimics phosphate except that arsenolysis by PNP is irreversible (*22*, *40*, *50*). KIEs were determined by the competitive radiolabeled method described previously (*22*, *38*, *40*, *50*). Briefly, V_{max}/K_m KIEs of all ^{3}H KIEs were measured using [5′-^{14}C]inosine as the remote label, while the other V_{max}/K_m KIEs were determined with [5′-$^3H_2$]inosine as the remote label. Each assay was performed in a total volume of 250 μL containing 1 nM enzyme and 250 μM substrate (at least 5×10^4 cpm for ^{14}C and 3:1 for ^{3}H:^{14}C cpm). A portion of the reaction mixture (50 μL) was allowed to reach 100% completion by adding another 5 nM enzyme and further incubating overnight, while the remaining 200 μL was quenched by heating to 95 °C for 3 min upon 20−30% completion. The reaction mixture was loaded onto charcoal-cellulose columns (4:1, 100 mg total, pre-equilibrated with 10 mM D-ribose) followed by washing with 100 μL of 10 mM D-ribose. The radiolabeled products of the PNP reaction were eluted with 3 mL of 20 mM D-ribose containing 10% ethanol (v/v). The effluent was collected, dried by speedvac, dissolved in 200 μL of water and 20 mL of scintillation fluid. The samples were then counted for 10 cycles at 10 min per cycle (Wallac 1414 LSC, Perkin-Elmer) and averaged. At least six replicates were performed for each KIE measurement.

^{3}H and ^{14}C emissions for each sample were determined according to eqs 1 and 2 (*38*). The ^{14}C channel ratio was obtained by counting a [1′-^{14}C]ribose standard to determine the ratio between channel A and channel B. Channels A and B were set such that all ^{3}H counts appear in channel A and only ^{14}C counts appear in channel B. The ^{3}H:^{14}C ratio was

$$\text{cpm } (^3\text{H}) = \text{cpm}_{\text{channelA}} - \text{cpm}_{\text{channelB}} \times (^{14}\text{C channel ratio}) \quad (1)$$

$$\text{cpm } (^{14}\text{C}) = \text{cpm}_{\text{channelB}} \times (1 + {}^{14}\text{C channel ratio}) \quad (2)$$

determined for the partial and complete reactions and the KIEs were corrected for 0% reaction according to eq 3, where f is the fraction of reaction completion, R_f and R_0 are the ratios of heavy to light isotope at partial and 100% completion of reaction, respectively (*38*).

$$\text{KIE} = \frac{\ln(1-f)}{\ln\left(1 - f \times \frac{R_f}{R_0}\right)} \quad (3)$$

Measurement of Forward Commitment Factor. Forward commitment factor of E:R-HsPNP was determined by isotope trapping experiments from the fraction of enzyme-bound, product-generating inosine during the first several catalytic turnovers in the presence of excess unlabeled inosine and arsenate (*22*). Briefly, 10 μL reaction mixtures containing 30 μM E:R-HsPNP, 50 mM Tris-HCl (pH 7.5) and 150 μM [1′-^{14}C]inosine (at least 2×10^4 cpm) were preincubated for 10 s and then rapidly chased with a solution of 140 μL containing 50 mM cold inosine and 5−100 mM arsenate. The reactions were quenched after 2 s by adding 50 μL of 1 M HCl. This reaction mixture was then rapidly loaded onto a charcoal-cellulose column. The radiolabeled product was resolved from substrates and analyzed by scintillation counting. The forward commitment factor was determined by extrapolation to saturating arsenate concentration. Control experiments were carried out in the absence of arsenate and used as background correction for forward commitment.

RESULTS AND DISCUSSION

PNP Transition-State Structures. Approximately 60 candidate structures of PNP transition states were optimized at the B3LYP/6-31G (d, p) level by altering systematically N-ribosidic and $O^{phosphate}$-ribosidic bond distances as well as the 2′-C-*exo/endo* configuration (Experimental Procedures and Supporting Information). These optimized structures (Figure 3) served as a candidate library for potential E:R-HsPNP transition states. The KIEs for the transition-state candidates were calculated using ISOEFF98 at H1′, H2′, H5′, C1′ and N9 (*48*). On the basis of the characteristic [1′-^{14}C] KIEs as well as C1′−N9 and C1′−$O^{phosphate}$ distances, these transition-state structures were divided into the categories (Figure 1, Figure 3 and Supporting Information) (i) *early*

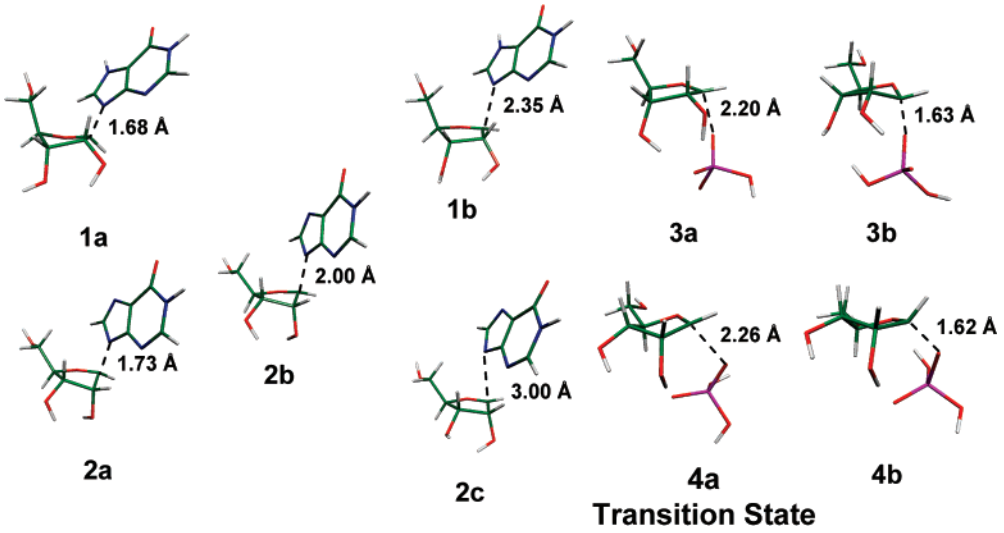

FIGURE 3: Representative structure candidates of PNP transition states. Approximately 60 candidate structures of PNP transition states were optimized *in vacuo* using hybrid density functional B3LYP/6-31G (d, p) methods implemented in Gaussian 98. The process of optimization started by systematically varying C1′−N9 or C1′−$O^{phosphate}$ bond distances as well as ribosyl pucker configuration and N7-protonation states. The C2′−C1′−N9−C2 dihedral angle was restricted to be 41° and the C5′-OH configuration of HsPNP (O5′−C5′−C4′−O4′ dihedral angle = 60°) was adopted as discussed in Experimental Procedures. Nine representative structures are shown with **1a** as an early dissociative $D_N^{\ddagger}*A_N$ transition state with N7-protonation, **1b** as a late dissociative $D_N^{\ddagger}*A_N$ transition state with N7-protonation, **2a** as an early dissociative $D_N^{\ddagger}*A_N$ transition state without N7-protonation, **2b** for a boundary structure between early and late dissociative $D_N^{\ddagger}*A_N$ transition states without N7-protonation, **2c** for a late dissociative $D_N^{\ddagger}*A_N$ transition state without N7-protonation, **3a** for an early associative $D_N*A_N^{\ddagger}$ transition state with C2′-*endo* configuration, **3b** for a late associative $D_N*A_N^{\ddagger}$ transition state with C2′-*endo* configuration, **4a** for an early associative $D_N*A_N^{\ddagger}$ transition state with C2′-*exo* configuration and **4b** for a late associative $D_N*A_N^{\ddagger}$ transition state with C2′-*exo* configuration, respectively. The computational KIEs of **4a** best match the intrinsic KIEs of E:R-HsPNP and thus the structure **4a** approximates the transition state of E:R-HsPNP.

dissociative $D_N^{\ddagger}*A_N$ transition states with significant [1′-^{14}C] KIEs and residual C1′−N9 bond order (distances < 2.3 Å) and no phosphate participation (such as **1a**, **2a** and **2b** in Figure 3); (ii) *late* dissociative $D_N^{\ddagger}*A_N$ transition states with [1′-^{14}C] KIEs near unity, C1′−N9 distances ≥ 2.3 Å and no phosphate participation (such as **1b** and **2c** in Figure 3); (iii) fully dissociative D_N*A_N (S_N1) transition states with no significant [1′-^{14}C] KIEs and without hypoxanthine and phosphate participation (*22*); (iv) *early* associative $D_N*A_N^{\ddagger}$ transition states with significant [1′-^{14}C] KIEs and C1′−$O^{phosphate}$ distances > 2.2 Å and no hypoxanthine participation (such as **3a**, **4a** in Figure 3); (v) *late* associative $D_N*A_N^{\ddagger}$ transition states with substantial [1′-^{14}C] KIEs and C1′−$O^{phosphate}$ distances ≤ 2.2 Å and no hypoxanthine participation (such as **3b**, **4b** in Figure 3). HsPNP has a *fully* dissociative D_N*A_N (S_N1) transition state and BtPNP adopts an *early* dissociative $D_N^{\ddagger}*A_N$ transition state. This global search for KIE-matched transition-state structure is useful to locate the nature of diverse transition states.

The C5′-OH configuration of HsPNP (O5′−C5′−C4′−O4′ dihedral angle = 60°) was used for transition-state optimization because HsPNP and E:R-HsPNP report the same 5′-^{3}H KIEs of 1.063 (Figure 4) (*47*). In comparison to free inosine, the hypoxanthine ring at the transition states is rotated toward the 2′-H with a C2′−C1′−N9−C2 dihedral angle of 41°, based on the structure of PNP bound to immucillin-H (see Experimental Procedures) (*47*). For N7-protonated $D_N^{\ddagger}*A_N$ transition states, both C2′-*exo* and *endo* conformations are allowed in the full range of C1′−N9 distances (≥1.8 Å). However, N7-unprotonated $D_N^{\ddagger}*A_N$ transition states favor C2′-*exo* configuration with a wide range of C1′−N9 distances. In contrast, the C2′-*endo* conformers are more favored for late dissociative $D_N^{\ddagger}*A_N$ transition states. Other N7-unprotonated, C2′-*endo* $D_N^{\ddagger}*A_N$

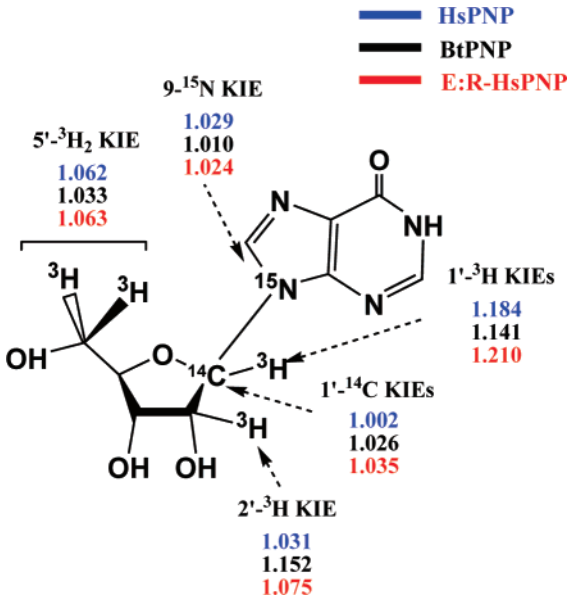

FIGURE 4: Intrinsic KIEs of HsPNP, BtPNP and E:R-HsPNP. The isotopically labeled positions are indicated in inosine. The intrinsic KIEs of E:R-HsPNP are from this work. Intrinsic KIEs of BtPNP and HsPNP have been reported previously (*21*, *22*). E:R-HsPNP shows both large [1′-^{3}H] and [1′-^{14}C] KIEs in comparison to HsPNP and BtPNP.

structures converged as C2′-*exo* isomers upon modeling. The instability of these N7-unprotonated C2′-*endo* structures is caused by gauche repulsion between 2′-H and C1′−N9 electrons, and is released by adopting the C2′-*exo* configuration or N7 protonation. For $D_N*A_N^{\ddagger}$ transition states, both C2′-*exo* and C2′-*endo* configurations are allowed for C1′−$O^{phosphate}$ distances between 1.8 Å and 2.8 Å. When the C1′−$O^{phosphate}$ ≥ 2.8 Å, C2′-*endo* conformers are preferred due to

Table 1: Apparent KIEs, Intrinsic KIEs and Computational KIEs of E:R-HsPNP[a]

		apparent KIEs,[c] intrinsic KIEs[d] and computational KIEs[e] of E:R-HsPNP			
inosine pairs[b]	type of KIEs	exptl KIEs[f]	apparent KIEs	intrinsic KIEs	computational KIEs
[1′-^{3}H] vs [5′-^{14}C]	α-secondary ^{3}H	1.170 ± 0.003	1.170 ± 0.003	1.210 ± 0.003	1.276
[2′-^{3}H] vs [5′-^{14}C]	β-secondary ^{3}H	1.061 ± 0.003	1.061 ± 0.003	1.075 ± 0.003	1.058
[1′-^{14}C] vs [5′-^{3}H$_2$]	primary ^{14}C	0.978 ± 0.002	1.028 ± 0.004	1.035 ± 0.005	1.035
[9-^{15}N, 5′-^{14}C] vs [5′-^{3}H$_2$]	primary ^{15}N	0.970 ± 0.003	1.020 ± 0.005	1.024 ± 0.005	1.027[g]
[9-^{15}N, 1′-^{14}C] vs [5′-^{3}H$_2$]	primary ^{14}C^{15}N	1.002 ± 0.002	1.053 ± 0.004	1.065 ± 0.005	1.062
[9-^{15}N, 1′-^{14}C] calcd[h]	primary ^{14}C^{15}N	0.949 ± 0.005	1.049 ± 0.009	1.060 ± 0.010	1.062
[5′-^{3}H$_2$] vs [5′-^{14}C][i]	remote ^{3}H	1.051 ± 0.002	1.051 ± 0.002	1.063 ± 0.002	1.107 (*proR & S*) 1.026 (*proR*) 1.078 (*proS*)

[a] The KIEs of E:R-HsPNP were measured or calculated as described in Experimental Procedures. [b] The first labels are for *V/K* KIEs, and the second are remote labels. [c] The apparent KIEs were obtained after correcting for the remote [5′-^{14}C] or [5′-^{3}H$_2$] KIEs, and corrections to 0% reaction, respectively. [d] The intrinsic KIEs were calculated from the apparent KIEs and forward commitment factor according to eq 5. [e] The computational KIEs were obtained on the basis of the vibrational modes of B3LYP/6-31G (d, p)-optimized E:R-HsPNP substrate and transition state using the ISOEFF98 program. [f] At least 6 measurements were made for each experimental KIE, and standard errors are calculated from the variation between experiments. [g] The [9-^{15}N] KIE is reported as the maximal [9-^{15}N] KIE for N7-protonated $D_N^{\ddagger}$*A_N transition states (Figure 7a) and is assumed to be the same as that at the N7-protonated D_N*$A_N^{\ddagger}$ transition state of E:R-HsPNP, because hypoxanthine N9 in both cases is more than 3.0 Å away from the anomeric carbon. [h] Calculated from the product of the [1′-^{14}C] and [9-^{15}N] KIEs. [i] This remote ^{3}H KIE arises from C−H distortion at the transition states. KIEs of *pro-R* and *pro-S* ^{3}H were calculated separately and are reported together as the [5′-^{3}H$_2$] KIE.

the favorable hyperconjugation between the C1′-H2′ σ bond and the anomeric carbon 2p$_z$ orbital (see discussion below). The C2′ geometry influences only the H-2′ KIE values. Consequently, only the C2′-geometry corresponding to the [2′-^{3}H] KIEs is discussed.

Apparent KIEs, Remote Label KIEs, Commitment to Catalysis and Intrinsic KIEs. The apparent KIE values for [1′-^{3}H], [2′-^{3}H], [5′-^{3}H$_2$], [1′-^{14}C], [9-^{15}N], and [1′-^{14}C, 9-^{15}N] inosines with E:R-HsPNP were determined by the competitive radiolabeled method (*22*, *47*). $^3(V_{max}/K_m)$ of 1.170 ± 0.003 for [1′-^{3}H], 1.061 ± 0.003 for [2′-^{3}H] and 1.051 ± 0.002 for [5′-^{3}H$_2$] were obtained using [1′-^{3}H]-, [2′-^{3}H]-, [5′-^{3}H$_2$]inosine as the isotope-labeled reactants and [5′-^{14}C]-inosine as the remote label, respectively (Table 1). The remote ^{14}C KIE is assumed to be unity because inosine [5′-^{14}C] is three bonds away from the N-ribosidic reaction center and ^{14}C KIE is insensitive to geometric variation in transition states (*22*, *38*, *39*). $^{14}(V_{max}/K_m)$, $^{15}(V_{max}/K_m)$ and $^{14,15}(V_{max}/K_m)$ for [1′-^{14}C], [9-^{15}N] and [1′-^{14}C, 9-^{15}N] were measured with [5′-^{3}H$_2$]inosine as the remote label and corrected for the 5.1% KIE of remote [5′-^{3}H$_2$] (Table 1). A similar [5′-^{3}H$_2$] KIE has been observed for HsPNP, consistent with C5′−H5′ bond distortion on forming the enzyme-bound transition state (*22*, *51*).

The observed V_{max}/K_m KIEs in competitive experiments include the contribution of forward and reverse commitments to catalysis and large commitments mask intrinsic KIEs (*22*, *38*, *39*). Intrinsic KIEs for E:R-HsPNP were obtained upon correcting for commitment factors according to eq 4 (Table 1), where $^H(V/K)$ is the observed heavy atom KIE, ^Hk is the intrinsic KIE, $^HK_{eq}$ is the equilibrium isotope effect between substrate and product, C_f and C_r are forward and reverse commitment, respectively, and H represents the heavy isotope ^{3}H, ^{14}C, or ^{15}N, respectively.

$$^H(V/K) = \frac{^Hk + C_f + C_r \times {}^HK_{eq}}{1 + C_f + C_r} \quad (4)$$

The forward commitment of E:R-HsPNP ($C_f = 0.239 \pm 0.025$) was obtained by the isotope trapping method (Figure 5). In contrast, HsPNP shows a smaller C_f of 0.147 (*22*). The 1.6-fold increase of C_f for E:R-HsPNP is caused by the K22E/H104R mutations, despite being over 25 Å from the enzyme active site (Figure 2). Since the change in K_m was modestly increased, C_f is likely to be from the increased k_{cat} (lowered transition-state barrier) for E:R-HsPNP (*30*). Arsenolysis prevents reverse commitment (C_r in eq 4) of E:R-HsPNP (*22*, *40*, *50*). Consequently, the intrinsic KIEs (^Hk) of [1′-^{3}H], [2′-^{3}H], [5′-^{3}H$_2$], [1′-^{14}C], [9-^{15}N], and [1′-^{14}C, 9-^{15}N] of E:R-HsPNP were derived from eq 5. Correction for forward commitment alters the apparent V_{max}/K_m KIEs to give intrinsic V_{max}/K_m KIEs (Table 1).

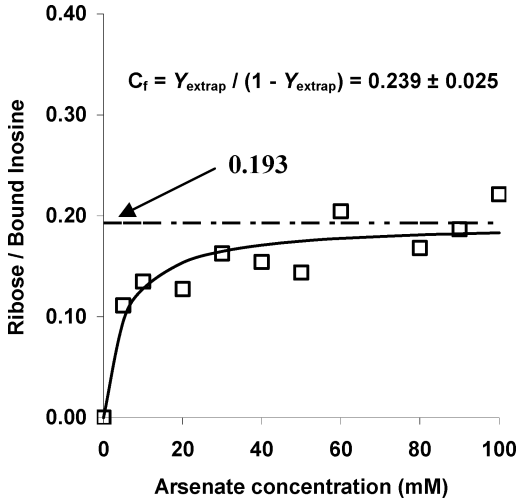

FIGURE 5: Measurement of forward commitment for E:R-HsPNP. Forward commitment was determined by isotope trapping experiments as described in Experimental Procedures. The *Y* axis intercept (Y_{extrap}) was obtained by extrapolating the molar ratio of ribose product to the initial enzyme−inosine complex under the condition of saturating arsenate. The forward commitment factor was calculated from the equation $C_f = Y_{extrap}/(1 - Y_{extrap})$.

$$^H(V/K) = \frac{^Hk + C_f}{1 + C_f} \quad (5)$$

Transition-State Structure of E:R-HsPNP. The intrinsic KIEs of E:R-HsPNP differ from both HsPNP and BtPNP

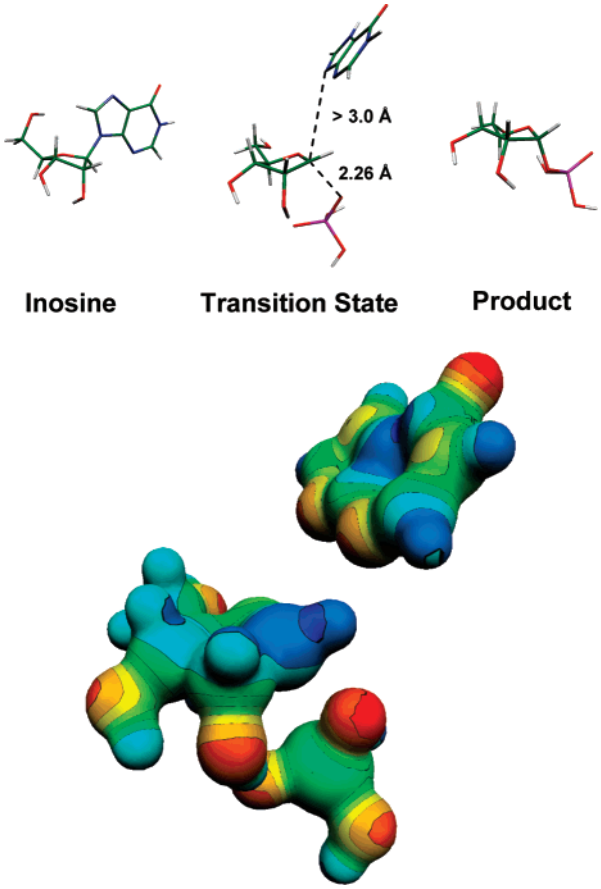

FIGURE 6: Structures of inosine, E:R-HsPNP transition state (TS) and ribose 1-phosphate product. The transition-state structure for E:R-HsPNP is shown with MEP and stick models. The N7-protonated hypoxanthine moiety was adapted from the corresponding $D_N^{\ddagger}*A_N$ transition-state structure whose C1′−N9 distance is at least 3.2 Å. The transition-state structure was optimized using hybrid density functional theory at the B3LYP/6-31G (d, p) level. Its KIE values match the intrinsic KIEs of E:R-HsPNP. The energy-minimized structures of inosine and ribose 1-phosphate were obtained with the same computational parameters. The CUBE subprogram of Gaussian 98 was used to generate molecular electrostatic potential (MEP) surfaces, which are visualized using Molekel 4.0.

(Figure 4) (*21*, *22*), establishing an altered transition state. Particularly, E:R-HsPNP exhibits larger [1′-^{3}H] and [1′-^{14}C] KIEs in comparison to HsPNP and BtPNP (Figure 4 and Table 1). Large [1′-^{14}C] KIEs can stem from the participation of either the leaving group or the nucleophile with C1′ at the transition state (*21*, *22*, *39*, *40*). The intrinsic KIEs were used as boundary constraints for comparison with the computational KIEs derived from the B3LYP-optimized transition-state structures with C1′−N9 and C1′−O^{phosphate} distances, ribosyl pucker configurations and N7-protonation states as variables. The transition-state structure of E:R-HsPNP (Figure 6 and Table 1) is in agreement with the intrinsic [1′-^{3}H], [2′-^{3}H], [1′-^{14}C] and [9-^{15}N] KIEs and shows the loss of the N-ribosidic bond (C1′−N9 distance ≥ 3.0 Å) and partial attack of nucleophilic phosphate (C1′−O^{phosphate} distance = 2.26 ± 0.02 Å). N7 of the leaving hypoxanthine at the transition state is fully protonated, and the ribosyl pucker is C2′-*exo*. The vector of the 5′-O→H bond is oriented away from the ribosyl group (Figure 3). The primary [1′-^{14}C] and [9-^{15}N] KIEs are key parameters for the determination of C1′−N9 and C1′−O^{phosphate} bond distances at the transition state. The large secondary [1′-^{3}H] KIE supports the dissociative character of the E:R-HsPNP transition state. β-Secondary [2′-^{3}H] and remote [5′-^{3}H$_2$] KIEs provide information on ribosyl ring pucker and 5′-OH configuration.

Remote [5′-^{3}H$_2$] KIE. The tritiums of [5′-^{3}H$_2$]inosine are four bonds away from the reaction center and are expected to be insensitive to the chemistry at the [1′-^{14}C] reaction center (*39*, *50*, *51*). Therefore, the intrinsic [5′-^{3}H$_2$] KIE of 1.063 ± 0.002 reports on the geometrical distortion of these bonds at the transition state. Significant remote [5′-^{3}H$_2$] KIEs have also been reported for HsPNP, BtPNP and PfPNP (*21*, *22*). Computational modeling indicates that isotope effects as large as 10% can be caused by altering the O5′−C5′−C4′−O4′ dihedral angle from − 55° for free inosine to 60° at the transition state. Of this 10% isotope effect, 2% and 8% are contributed from the [5′-^{3}H-*proR*] and [5′-^{3}H-*proS*] positions, respectively. The [5′-^{3}H$_2$] KIE of 1.063 ± 0.002 with E:R-HsPNP is slightly lower than the calculated value (Table 1), however, KIEs calculated for ^{3}H *in vacuo* tend to be overestimated because van der Waals interactions at enzyme active sites might restrict the out-of-plane bending motions (*22*, *39*−*41*). The hydrogen bond between the 5′-OH and PNP His257 is responsible for the energetically unfavorable 5′-OH orientation (*47*). It is possible that bond bending at the transition state can further contribute to the observed ^{3}H KIEs. It may account for the slight difference between the experimental and the calculated ^{3}H KIEs.

α-*Secondary [1′-^{3}H] KIE*. A large α-secondary [1′-^{3}H] KIE is indicative of C1′ sp^2 hybridization at the transition state, whereas a near unity α-secondary [1′-^{3}H] KIE corresponds to more sp^3 character for C1′ at the transition state (Figure 1 and Supporting Information) (*21*, *22*, *40*, *41*). The intrinsic [1′-^{3}H] KIE of 1.210 ± 0.003 (Table 1) is consistent with dissociative or early associative transition states. The E:R-HsPNP [1′-^{3}H] KIE is larger than those of HsPNP and BtPNP (Figure 4) (*21*, *22*). Thus the transition state of E:R-HsPNP has more freedom in the H1′ vibrational modes than the transition states for HsPNP and BtPNP (*22*, *39*, *41*). The C1′−H1′ out-of-plane bending mode is highly sensitive to the C1′−N9 distance and to nucleophilic participation. Although the computational [1′-^{3}H] KIE of 1.298 for E:R-HsPNP transition state is slightly higher than the experimentally obtained intrinsic [1′-^{3}H] KIE of 1.210 ± 0.003 (Table 1), computational β-secondary [1′-^{3}H] KIEs are commonly overestimated by *in vacuo* calculations (*22*, *26*, *41*). This limitation may reflect van der Waals interactions that suppress out-of-plane bending motions of C−H bonds at the catalytic sites.

Primary [9-^{15}N] KIE. The primary [9-^{15}N] KIE reports the loss of C1′−N9 bond order as well as the rehybridization of hypoxanthine at the transition state. In addition, the protonation state of purine ring nitrogens at the transition state is reflected in the [9-^{15}N] KIE. The [9-^{15}N] KIE of 1.024 ± 0.005 for E:R-HsPNP (Table 1) is consistent with complete dissociation of the N-ribosidic bond (at least 3.0 Å and less than 0.02 Pauling bond order) and N7 protonation of the leaving hypoxanthine moiety at the transition state (Figure 6). Computational modeling results show that [9-^{15}N] KIEs for N7-protonated PNP transition states increase from unity to 1.027 as the C1′−N9 distances vary from 1.46 Å for full-bond-order substrate to ≥3.0 Å for a fully dissociative

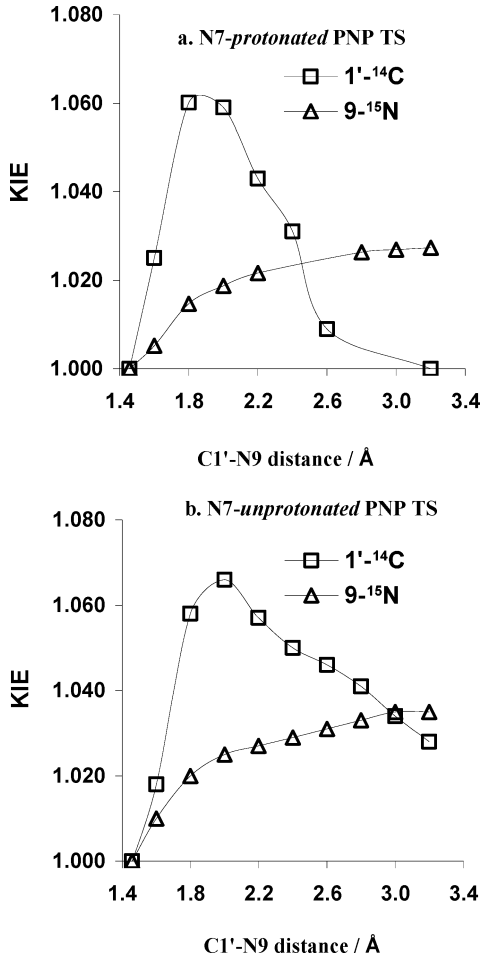

FIGURE 7: Computational [1′-^{14}C] and [9-^{15}N] KIEs for inosine at dissociative transition states with varied C1′−N9 distances. Transition-state structures were optimized *in vacuo* using hybrid density functional theory implemented in Gaussian 98 at the B3LYP/6-31G (d, p) level. The process started by systematically varying C1′−N9 distances as well as ribosyl pucker and N7-protonation. The orientations of C5′-OH and purine were restricted to those found in PNP crystal structures as described in Experimental Procedures. The KIEs were calculated using the ISOEFF98 program. The C2′-*exo* and C2′-*endo* isomers with the same N7 protonation state and C1′−N9 distances report almost identical KIEs except at the H2′ position. The KIEs of C2′-*endo* isomers are shown here because they are a better match to the [2′-^{3}H] KIE of E:R-HsPNP. Complete [1′-^{14}C] KIEs for N7-unprotonated dissociative transition states reach unity only when C1′−N9 distances are more than 4.0 Å (*41*): (a) N7-protonated transition states and (b) N7-unprotonated transition states.

oxacarbenium ion intermediate (Figure 7a). Given the intrinsic errors of KIE measurements (Table 1) and the insensitivity of [9-^{15}N] KIE in the range of large C1′−N9 distances (the plateau in Figure 7a,b), [9-^{15}N] KIE of 1.024 ± 0.005 together with the modest-to-large [2′-^{3}H] (discussion below) and [1′-^{3}H] KIEs (discussion above) led to a C1′−N9 distance ≥3.0 Å at the transition state. We also calculated [9-^{15}N] KIEs for *N7-unprotonated* PNP transition states as a function of C1′−N9 distances (Figure 7b). Although a N7-*unprotonated* transition-state candidate (**2b**) with C1′−N9 distance of 2.0 Å matches the intrinsic KIE of 1.024 ± 0.005, the calculated [1′-^{14}C] KIE of 1.060 for such a structure is significantly larger than the experimental KIE of 1.035 (see discussion below and Table 2). The primary [9-^{15}N] KIE of 1.024 ± 0.005, together with the primary [1′-^{14}C] KIE of 1.035 (see discussion below), supports N7 protonation at the transition state. Similar primary [9-^{15}N] KIEs between E:R-HsPNP and HsPNP (1.024 ± 0.005 vs 1.029 ± 0.006) argue that the two transition states are similar in regard to hypoxanthine dissociation and N7 protonation (*21*, *22*). The transition state of HsPNP has been characterized as N7-protonated with full loss of the C1′−N9 bond (*22*).

Primary [1′-^{14}C] and [1′-^{14}C, 9-^{15}N] KIEs. The primary ^{14}C KIE is highly informative for determining transition-state structures in nucleophilic substitution reactions (*21*, *22*, *40*, *50*). Unity or slightly inverse [1′-^{14}C] KIEs are observed for complete dissociative D_N*A_N transition states (*39*). For borderline S_N1 reactions, [1′-^{14}C] KIE is expected to be in the range of 1.01−1.06 (Figure 1) (*39*). The [1′-^{14}C] KIE of 1.035 ± 0.005 for E:R-HsPNP is consistent with a mechanism in which N-ribosidic bond dissociation is rapid and attack of the nucleophilic arsenate provides the highest barrier transition state on the reaction coordinate (Figure 1). The computationally matched KIEs indicate a C1′−O^{phosphate} bond distance of 2.26 Å with a Pauling bond order of 0.1 at the transition state. Several other transition states (Figure 6) also predict a primary [1′-^{14}C] KIE of 1.035 (Table 2). These structures have either significant N9−C1′ bond order or short C1′−O^{phosphate} distances and can be eliminated because their KIEs at other positions do not agree with the intrinsic KIEs (Figure 3, Table 2).

The C1′−N9 and C1′−O^{phosphate} bond distances were determined primarily from the [1′-^{14}C] and [9-^{15}N] KIEs of E:R-HsPNP. The certainty of the transition state is subject to the accuracy of these primary KIEs. Given the intrinsic errors for [1′-^{14}C] and [9-^{15}N] as well as the relatively large 6.3% KIE for the [5′-$^{3}H_2$] remote label, we also measured the primary [1′-^{14}C, 9-^{15}N] KIE as a parallel control. The [1′-^{14}C, 9-^{15}N] KIE of 1.065 ± 0.005 showed good agreement with the product (1.060) of the individual primary [1′-^{14}C] KIE of 1.035 ± 0.005 and [9-^{15}N] KIE of 1.024 ± 0.005 (Table 1).

β-Secondary [2′-^{3}H] KIE. The β-secondary [2′-^{3}H] KIE is influenced by the degree of hyperconjugation between the C1′-H2′ σ bond and the anomeric carbon 2p_z orbital (*22*, *39*). The magnitude of the KIE is proportional to (i) the dihedral angle between the C1′−H2′ σ bond and the anomeric 2p_z orbital and (ii) the degree of C1′−N9 and C1′−O^{phosphate} bond dissociation (*22*, *39*). These factors are also correlated to ribosyl ring pucker and N9−C1′, C1′−O^{phosphate} bond distances at the transition state. A large β-secondary [2′-^{3}H] KIE is consistent with complete dissociation of the leaving group, insignificant participation of the nucleophile and a $\cos^2\theta = 1$ H2′−C2′−C1′−p_z(C1′) dihedral angle. In contrast, small β-secondary [2′-^{3}H] KIEs correspond to significant participation of the leaving group or nucleophile, or close to 90° ($\cos^2\theta = 0$) H2′−C2′−C1′-p_z dihedral angle. Consequently, β-secondary [2′-^{3}H] KIEs are useful for determining C1′−N9 and C1′−O^{phosphate} bond distances as well as ribosyl pucker at transition states. The modest intrinsic [2′-^{3}H] KIE of 1.075, together with a [1′-^{14}C] KIE of 1.035 for E:R-HsPNP, agrees with the computational KIEs of 1.057 and 1.035, respectively, for the proposed E:R-HsPNP transition state with C1′−O^{phosphate} bond = 2.26 Å (Figure 6 and Table 1). This transition state adopts a C2′-*exo* configuration with the dihedral angles of H2′−C2′−C1′−p_z(C1′) and H2′−C2′−C1′−O^{phosphate} of 70° and 110°, respectively. The corresponding C2′-*endo* conformer (**3a**)

Table 2: Comparison between Intrinsic KIEs and Computational KIEs[a]

		computational KIEs[b]								
		dissocative transition states[d]					associative transition states[d]			
		N7-protonated		N7-unprotonated			2′-H-*endo*		2′-H-*exo*	
type of KIEs	intrinsic KIEs[c]	**1a**[e]	**1b**[e]	**2a**[e]	**2b**[f]	**2c**[e]	**3a**[e]	**3b**[e]	**4a**[g]	**4b**[e]
primary 1′-^{14}C	1.035	1.034	1.033	1.032	1.066	1.034	1.035	1.032	1.035	1.033
primary [h] 9-^{15}N	1.024	1.009	1.023	1.016	1.025	1.035	1.027(35)	1.027(35)	1.027(35)	1.027(35)
α-secondary 1′-^{3}H	1.210	1.063	1.314	1.093	1.201	1.489	1.288	1.063	1.276	1.024
β-secondary 2′-^{3}H	1.075	0.984	1.006	0.942	0.938	1.104	1.180	1.067	1.058	1.004
remote 5′-^{3}H	1.063	1.075	1.020	1.071	1.060	1.026	1.105	1.101	1.107	1.080

[a] The computational KIEs of the E:R-HsPNP transition state and nine representative PNP transition states are compared with the intrinsic KIEs of E:R-HsPNP. All transition states in this table show partial matched KIEs in comparison to the intrinsic KIEs of E:R-HsPNP. The structures are shown in Figure 3. [b] The computational KIEs were calculated using ISOEFF98 program on the basis of the optimized PNP transition-state structures in Figure 3. [c] The intrinsic KIEs were measured by the competitive radiolabeled method as described in Experimental Procedures and shown in Table 1. [d] Dissociative and associative transition states are defined in Figures 1 and 6. [e] Transition-state structures with matched [1′-^{14}C] KIE in comparison with E:R-HsPNP. [f] Transition-state structures with matched [9-^{15}N] KIE in comparison with E:R-HsPNP. [g] The transition-state structure solved for E:R-HsPNP. [h] Two sets of [9-^{15}N] KIEs are reported for associative transition states with 1.027 for N7-protonated hypoxanthine and 1.035 for N7-unprotonated hypoxanthine at the transition states, respectively. The values are estimated on the basis of maximal [9-^{15}N] KIEs for the fully dissociative transition states, where hypoxanthine is at least 3.0 Å away from anomeric carbon and thus is assumed to report the same [9-^{15}N] KIEs as for associative transition states.

predicts a KIE of 1.20 (Figure 8 and Table 2). In addition, the [2′-^{3}H] KIE rules out the possibility that E:R-HsPNP adopts an early dissociative transition state, because none of these reported structures match both [1′-^{14}C] and [2′-^{3}H] KIEs (Table 2). Consequently, primary [1′-^{14}C] and [1′-^{15}N] KIEs, together with secondary [1′-^{3}H] and [2′-^{3}H], define the early associative character of the E:R-HsPNP transition state (Figure 6 and Table 2).

Comparative Transition States of HsPNP, BtPNP and E:R-HsPNP. The transition-state structures of HsPNP and BtPNP have been reported previously (*21*, *22*). Although these PNPs share 87% amino acid sequence identity, their transition-state structures are different. HsPNP has a fully dissociative transition state where both leaving hypoxanthine and nucleophilic arsenate have no participation and an oxacarbenium ion intermediate is formed (*22*). The dissociative character of the HsPNP transition state is reflected by unity [1′-^{14}C] and large [9-^{15}N] KIEs of 1.002 and 1.029, respectively (Figure 4). In contrast, BtPNP features an early dissociative transition state with a significant C1′−N9 bond order and short C1′−N9 distance of 1.8 Å (*21*, *22*). The proposed transition-state structure of BtPNP is consistent with a small [9-^{15}N] KIE of 1.010 and modest [1′-^{14}C] of 1.026 (Figure 4). E:R-HsPNP is a chimeric HsPNP containing K22E/H104R mutations found in BtPNP incorporated into its primary amino acid sequence. These changes make the transition state of E:R-HsPNP different from either parent. It is more similar to that of human 5′-methylthio adenosine phosphorylase (*40*) than to HsPNP or BtPNP (*21*, *22*). Enzymatic transition states from KIE analysis report on the rate-determining chemical step along the reaction coordinate. Consequently, C1′−N9 bond dissociation, oxacarbenium ion intermediate formation and C1′−O^{phosphate} bond formation are possible transition state features of the PNPs. Notably, BtPNP-, HsPNP- and E:R-HsPNP-catalyzed arsenolysis each show different feature along the reaction coordinate as the transition-state structure. This observation is remarkable since E:R-HsPNP and HsPNP differ only by two residues that are 25 Å away from their active sites (Figure 2). The variation among BtPNP, HsPNP and E:R-HsPNP transition states argues that the K22E/H104R double mutant transmits key transition-state stabilization from BtPNP to HsPNP.

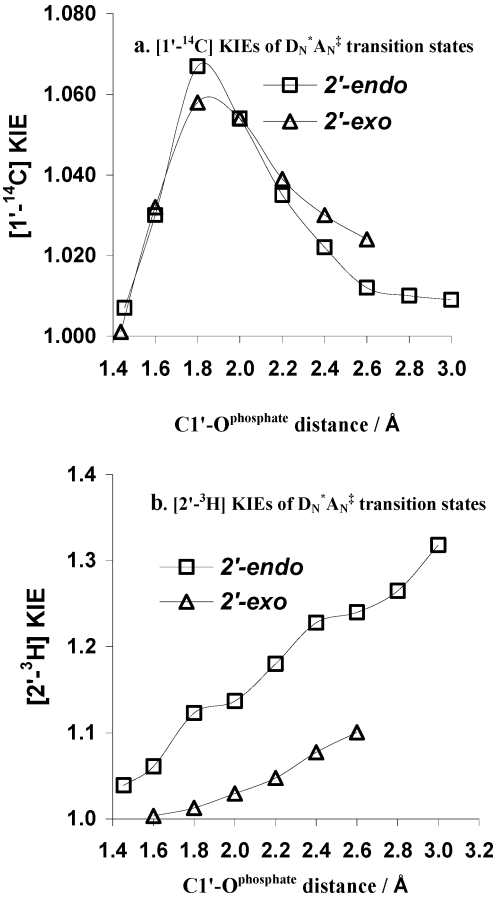

FIGURE 8: Computational [1′-^{14}C] and [2′-^{3}H] KIEs for inosine at late PNP D_N*A_N‡ transition states with varied C1′−O^{phosphate} distances. The structures of D_N‡*A_N transition states were optimized as described in Figure 7. C1′−O^{phosphate} distances as well as the ribosyl configuration were varied with the C5′-OH orientation restricted. The KIEs of optimized structures were calculated using ISOEFF98. For C1′−O^{phosphate} distances between 1.6 Å and 2.8 Å, both C2′-*exo* and C2′-*endo* conformers are stable. In contrast, C2′-*endo* conformers are preferred for C1′−O^{phosphate} ≥ 2.8 Å. For cases where C1′−O^{phosphate} ≥ 2.8 Å, only KIEs of the C2′-*endo* structures are plotted. (a) [1′-^{14}C] KIEs for C2′-*endo/exo* transition states and (b) [2′-^{3}H] KIEs for C2′-*endo/exo* transition states.

Effects of Remote Mutations on E:R-HsPNP Transition State and Reaction Profile. The reaction coordinates and

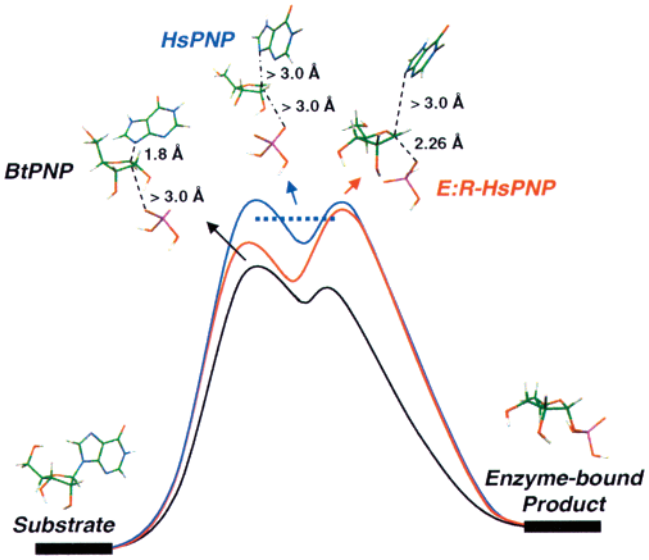

FIGURE 9: The reaction coordinates for inosine phosphorolysis catalyzed by HsPNP, BtPNP and E:R-HsPNP. The relative energy along the reaction coordinate is arbitrary with the highest energetic points as the chemical transition states. The first reaction barrier represents the dissociation of N-ribosidic bond, and the second barrier corresponds to the attack of phosphate. The ribooxacarbenium intermediate is between these transition states (dashed blue line). BtPNP has an early dissociative transition state (N-ribosidic bond dissociation, black trace). In contrast, the transition state of HsPNP features a relatively stable ribooxacarbenium intermediate. The rate-limiting chemical step of E:R-HsPNP is C1'−$O^{phosphate}$ bond formation. BtPNP stabilizes a lower energy transition state than HsPNP. A lower energy for oxacarbenium ion formation also occurs in the transition state for E:R-HsPNP. The subsequent C1′−$O^{phosphate}$ bond formation is the high-barrier transition state for E:R-HsPNP.

transition-state structures of BtPNP, HsPNP and E:R-HsPNP all follow a "nucleophilic displacement−electrophilic migration" mechanism but are distinguished from one another by the positions of their transition states along the reaction coordinate (Figures 1, 9). E:R-HsPNP is the first member of the PNPs that adopts an early nucleophilic transition state, for which C1′−N9 bond dissociation and ribooxacarbenium formation are rapid and the rate-limiting chemical step is the migration of the ribooxacarbenium ion coupled to attack of the nucleophilic arsenate. The transition state of BtPNP shows early dissociative character where the breaking of N-ribosidic bond is slow in comparison to the subsequent steps (*21*). In contrast, HsPNP forms a completely dissociated transition state as a ribooxacarbenium ion intermediate (*22*). The K22E/H104R double mutations in E:R-HsPNP alter the transition state of HsPNP by lowering the energy barrier for C1′−N9 bond dissociation on the path to formation of the oxacarbenium ion intermediate. This stabilization in E:R-HsPNP causes the C1′−$O^{phosphate}$ association step to be the transition state barrier along the reaction profile (Figure 9). Pre-steady-state kinetic data show that the chemical step of BtPNP-catalyzed inosine phosphorolysis is more rapid than that of HsPNP (*30*). This rate acceleration argues for better stabilization at the transition state of BtPNP than for HsPNP. Aspects of the favorable transition-state formation in BtPNP are transferred to E:R-HsPNP via the K22E/H104R mutations. A computational study, using QM/MM analysis has proposed that the remote K22E/H104R mutations in E:R-HsPNP facilitate nucleoside phosphorolysis via dynamic coupling at the enzyme active sites.[3] Favorable partition of the Michaelis complex toward the transition state is consistent with the increase in forward commitment factor in E:R-HsPNP (*22*, *39*). Consequently, the double mutations in E:R-HsPNP facilitate rapid formation of the oxacarbenium ion species to make C1′−$O^{phosphate}$ bond association the dominant transition state.

CONCLUSION

E:R-HsPNP is a bovinized mutant of HsPNP achieved by replacing its K22 and H104 with the corresponding Glu and Arg residues of BtPNP. The transition-state structure of E:R-HsPNP was solved by competitive KIEs and density functional calculations. The transition-state candidates were optimized with respect to C1′−N9 and C1′−$O^{phosphate}$ distances, ribosyl configurations, N7-protonation states and 5′-OH geometry. The E:R-HsPNP transition state features a C2′-*exo*-ribosyl ring pucker, a fully dissociative, N7-protonated hypoxanthine, and weak participation of the arsenate nucleophile. This early associative transition state of E:R-HsPNP is distinguished from early and fully dissociative transition states of BtPNP and HsPNP, respectively. The alteration of the transition-state structures from HsPNP to E:R-HsPNP is remarkable, because the two enzymes are different from each other by only two residues that are at least 25 Å from the enzyme active site. The remote K22E/H104R mutations lower the energy (increase the probability) for N-ribosidic bond breaking and thus leave the later C1′−$O^{phosphate}$ bond formation as the transition state for catalysis by E:R-HsPNP. This systematic approach for solving the E:R-HsPNP transition state provides a candidate library of PNP transition states that can be used as a benchmark for transition-state characterization of other PNPs and N-ribosyl transferase enzymes.

ACKNOWLEDGMENT

The authors thank Prof. Jiali Gao in Department of Chemistry at University of Minnesota for allocation of time for Gaussian calculations at the Minnesota Supercomputer Institute.

SUPPORTING INFORMATION AVAILABLE

Full author list of ref *46* and complete calculation results. This material is available free of charge via the Internet at http://pubs.acs.org.

REFERENCES

1. Kim, B. K., Cha, S., and Parks, R. E., Jr. (1968) Purine nucleoside phosphorylase from human erythroyctes. II. Kinetic analysis and substrate-binding studies, *J. Biol. Chem. 243*, 1771−1776.
2. Gelfand, E. W., Dosch, H. M., Biggar, W. D., and Fox, I. H. (1978) Partial purine nucleoside phosphorylase deficiency. Studies of lymphocyte function, *J. Clin. Invest. 61*, 1071−1080.
3. Gelfand, E. W., Fox, I. H., Stuckey, M., and Dosch, H. M. (1978) Normal B-lymphocyte function in patients with Lesch-Nyhan syndrome and HGPRT deficiency, *Clin. Exp. Immunol. 31*, 205−208.
4. Giblett, E. R., Ammann, A. J., Wara, D. W., Sandman, R., and Diamond, L. K. (1975) Nucleoside-phosphorylase deficiency in

a child with severely defective T-cell immunity and normal B-cell immunity, *Lancet 1*, 1010−1013.
5. Bzowska, A., Kulikowska, E., and Shugar, D. (2000) Purine nucleoside phosphorylases: properties, functions, and clinical aspects, *Pharmacol. Ther. 88*, 349−425.
6. Kicska, G. A., Long, L., Horig, H., Fairchild, C., Tyler, P. C., Furneaux, R. H., Schramm, V. L., and Kaufman, H. L. (2001) Immucillin H, a powerful transition-state analog inhibitor of purine nucleoside phosphorylase, selectively inhibits human T lymphocytes, *Proc. Natl. Acad. Sci. U.S.A. 98*, 4593−4598.
7. Schramm, V. L. (2004) Immucillins as antibiotics for T-cell proliferation and malaria, *Nucleosides, Nucleotides Nucleic Acids 23*, 1305−1311.
8. Schramm, V. L., and Grubmeyer, C. (2004) Phosphoribosyltransferose mechanisms and roles in nucleic acid metabolism, *Prog. Nucleic Acid Res. Mol. Biol. 78*, 261−304.
9. Taylor, E. A., Clinch, K., Kelly, P. M., Li, L., Evans, G. B., Tyler, P. C., and Schramm, V. L. (2007) Acyclic ribooxacarbenium ion mimics as transition state analogues of human and malarial purine nucleoside phosphorylases, *J. Am. Chem. Soc. 129*, 6984−6985.
10. Taylor Ringia, E. A., Tyler, P. C., Evans, G. B., Furneaux, R. H., Murkin, A. S., and Schramm, V. L. (2006) Transition state analogue discrimination by related purine nucleoside phosphorylases, *J. Am. Chem. Soc. 128*, 7126−7127.
11. Talyor Ringia, E. A., and Schramm, V. L. (2005) Transition states and inhibitors of the purine nucleoside phosphorylase family, *Curr. Top. Med. Chem. 5*, 1237−1258.
12. Schramm, V. L. (2005) Enzymatic transition states and transition state analogues, *Curr. Opin. Struct. Biol. 15*, 604−613.
13. Evans, G. B., Furneaux, R. H., Tyler, P. C., and Schramm, V. L. (2003) Synthesis of a transition state analogue inhibitor of purine nucleoside phosphorylase via the Mannich reaction, *Org. Lett. 5*, 3639−3640.
14. Evans, G. B., Furneaux, R. H., Lewandowicz, A., Schramm, V. L., and Tyler, P. C. (2003) Exploring structure-activity relationships of transition state analogues of human purine nucleoside phosphorylase, *J. Med. Chem. 46*, 3412−3423.
15. Evans, G. B., Furneaux, R. H., Lewandowicz, A., Schramm, V. L., and Tyler, P. C. (2003) Synthesis of second-generation transition state analogues of human purine nucleoside phosphorylase, *J. Med. Chem. 46*, 5271−5276.
16. Deng, H., Murkin, A. S., and Schramm, V. L. (2006) Phosphate activation in the ground state of purine nucleoside phosphorylase, *J. Am. Chem. Soc. 128*, 7765−7771.
17. Deng, H., Lewandowicz, A., Schramm, V. L., and Callender, R. (2004) Activating the phosphate nucleophile at the catalytic site of purine nucleoside phosphorylase: A vibrational spectroscopic study, *J. Am. Chem. Soc. 126*, 9516−9517.
18. Nunez, S., Antoniou, D., Schramm, V. L., and Schwartz, S. D. (2004) Promoting vibrations in human purine nucleoside phosphorylase. A molecular dynamics and hybrid quantum mechanical/molecular mechanical study, *J. Am. Chem. Soc. 126*, 15720−15729.
19. Deng, H., Cahill, S. M., Abad, J. L., Lewandowicz, A., Callender, R. H., Schramm, V. L., and Jones, R. A. (2004) Active site contacts in the purine nucleoside phosphorylase - Hypoxanthine complex by NMR and ab initio calculations, *Biochemistry 43*, 15966−15974.
20. Fedorov, A., Shi, W., Kicska, G., Fedorov, E., Tyler, P. C., Furneaux, R. H., Hanson, J. C., Gainsford, G. J., Larese, J. Z., Schramm, V. L., and Almo, S. C. (2001) Transition state structure of purine nucleoside phosphorylase and principles of atomic motion in enzymatic catalysis, *Biochemistry 40*, 853−860.
21. Kline, P. C., and Schramm, V. L. (1993) Purine nucleoside phosphorylase. Catalytic mechanism and transition-state analysis of the arsenolysis reaction, *Biochemistry 32*, 13212−13219.
22. Lewandowicz, A., and Schramm, V. L. (2004) Transition state analysis for human and *Plasmodium falciparum* purine nucleoside phosphorylases, *Biochemistry 43*, 1458−1468.
23. Mao, C., Cook, W. J., Zhou, M., Koszalka, G. W., Krenitsky, T. A., and Ealick, S. E. (1997) The crystal structure of *Escherichia coli* purine nucleoside phosphorylase: a comparison with the human enzyme reveals a conserved topology, *Structure 5*, 1373−1383.
24. Narayana, S. V. L., Bugg, C. E., and Ealick, S. E. (1997) Refined structure of purine nucleoside phosphorylase at 2.75 angstrom resolution, *Acta Crystallogr., Sect. D: Biol. Crystallogr. 53*, 131−142.
25. Mao, C., Cook, W. J., Zhou, M., Federov, A. A., Almo, S. C., and Ealick, S. E. (1998) Calf spleen purine nucleoside phosphorylase complexed with substrates and substrate analogues, *Biochemistry 37*, 7135−7146.
26. McCann, J. A., and Berti, P. J. (2007) Transition State Analysis of Acid-Catalyzed dAMP Hydrolysis, *J. Am. Chem. Soc. 129*, 7055−7064.
27. Luic, M., Koellner, G., Yokomatsu, T., Shibuya, S., and Bzowska, A. (2004) Calf spleen purine-nucleoside phosphorylase: crystal structure of the binary complex with a potent multisubstrate analogue inhibitor, *Acta Crystallogr., Sect. D: Biol. Crystallogr. 60*, 1417−1424.
28. de Azevedo, W. F., Jr., Canduri, F., dos Santos, D. M., Silva, R. G., de Oliveira, J. S., de Carvalho, L. P., Basso, L. A., Mendes, M. A., Palma, M. S., and Santos, D. S. (2003) Crystal structure of human purine nucleoside phosphorylase at 2.3Å resolution, *Biochem. Biophys. Res. Commun. 308*, 545−552.
29. Canduri, F., Fadel, V., Dias, M. V., Basso, L. A., Palma, M. S., Santos, D. S., and de Azevedo, W. F., Jr. (2005) Crystal structure of human PNP complexed with hypoxanthine and sulfate ion, *Biochem. Biophys. Res. Commun. 326*, 335−338.
30. Ghanem, M., Li, L., Wing, C., and Schramm, V. L. (2008) Altered thermodynamics from remote mutations altering human toward bovine purine nucleoside phosphorylase, *Biochemistry 47*, 2559−2564.
31. Cleland, W. W. (2005) The use of isotope effects to determine enzyme mechanisms, *Arch. Biochem. Biophys. 433*, 2−12.
32. Lewis, B. E., and Schramm, V. L. (2001) Conformational equilibrium isotope effects in glucose by C-13 NMR spectroscopy and computational studies, *J. Am. Chem. Soc. 123*, 1327−1336.
33. Gambogi, J. E., L'Esperance, R. P., Lehmann, K. K., Pate, B. H., and Scoles, G. (1993) The rate of intramolecular vibrational-energy relaxation of the fundamental C-H stretch in (CF3)3C-CC-H, *J. Chem. Phys. 98*, 1116−1122.
34. Cha, Y., Murray, C. J., and Klinman, J. P. (1989) Hydrogen tunneling in enzyme reactions, *Science 243*, 1325−1330.
35. Shiner, V. J. J. (1959) Deuterium isotope effects and hyperconjugation, *Tetrahedron 5*, 243−252.
36. Lewis, E. S. (1959) Isotope effects and hyperconjugation, *Tetrahedron 5*, 143−148.
37. Lewis, E. S., and Boozer, C. E. (1952) Isotope effects in the ionization of alkyl chlorosulfites, *J. Am. Chem. Soc. 74*, 6306−6307.
38. Luo, M., Singh, V., Taylor, E. A., and Schramm, V. L. (2007) Transition-State Variation in Human, Bovine, and *Plasmodium falciparum* Adenosine Deaminases, *J. Am. Chem. Soc. 129*, 8008−8017.
39. Singh, V., Lee, J. E., Nunez, S., Howell, P. L., and Schramm, V. L. (2005) Transition state structure of 5′-methylthioadenosine/S-adenosylhomocysteine nucleosidase from *Escherichia coli* and its similarity to transition state analogues, *Biochemistry 44*, 11647−11659.
40. Singh, V., and Schramm, V. L. (2006) Transition-state structure of human 5′-methylthioadenosine phosphorylase, *J. Am. Chem. Soc. 128*, 14691−14696.
41. Singh, V., and Schramm, V. L. (2007) Transition-state analysis of *S-pneumoniae* 5′-methylthioadenosine nucleosidase, *J. Am. Chem. Soc. 129*, 2783−2795.
42. Schramm, V. L. (2005) Enzymatic transition states: thermodynamics, dynamics and analogue design, *Arch. Biochem. Biophys. 433*, 13−26.
43. Schramm, V. L. (1999) Enzymatic transition-state analysis and transition-state analogs, *Methods Enzymol. 308*, 301−355.
44. Barrio, M. D., Scopes, D. I., Holtwick, J. B., and Leonard, N. J. (1981) Syntheses of all singly labeled [N]adenines: Mass spectral fragmentation of adenine, *Proc. Natl. Acad. Sci. U.S.A. 78*, 3986−3988.
45. Merkler, D. J., Kline, P. C., Weiss, P., and Schramm, V. L. (1993) Transition-state analysis of AMP deaminase, *Biochemistry 32*, 12993−13001.
46. Frisch, M. J., et al. (1998) *Gaussian 98*, Gaussian, Inc., Pittsburgh, PA.
47. Murkin, A. S., Birck, M. R., Rinaldo-Matthis, A., Shi, W., Taylor, E. A., Almo, S. C., and Schramm, V. L. (2007) Neighboring group

participation in the transition state of human purine nucleoside phosphorylase, *Biochemistry 46*, 5038−5049.
48. Anisimov, V., and Paneth, P. (1999) ISOEFF98. A program for studies of isotope effects using Hessian modifications, *J. Math. Chem. 26*, 75−86.
49. Mentch, F., Parkin, D. W., and Schramm, V. L. (1987) Transition-state structures for N-glycoside hydrolysis of AMP by acid and by AMP nucleosidase in the presence and absence of allosteric activator, *Biochemistry 26*, 921−930.
50. Birck, M. R., and Schramm, V. L. (2004) Nucleophilic participation in the transition state for human thymidine phosphorylase, *J. Am. Chem. Soc. 126*, 2447−2453.
51. Birck, M. R., and Schramm, V. L. (2004) Binding causes the remote [5′-^{3}H]thymidine kinetic isotope effect in human thymidine phosphorylase, *J. Am. Chem. Soc. 126*, 6882−6883.

BI702133X